Influence of strain on transport in dense Lennard-Jones systems

Janka Petravic

Citation: The Journal of Chemical Physics **120**, 7041 (2004); doi: 10.1063/1.1683073
View online: http://dx.doi.org/10.1063/1.1683073
View Table of Contents: http://scitation.aip.org/content/aip/journal/jcp/120/15?ver=pdfcov
Published by the AIP Publishing

Influence of strain on transport in dense Lennard-Jones systems

Janka Petravic
Research School of Chemistry, The Australian National University, Canberra ACT 0200, Australia

(Received 14 November 2003; accepted 22 January 2004)

We study the shear stress relaxation and temperature dependence of the diffusion coefficient, viscosity, and thermal conductivity along a high-density Lennard-Jones isochore of the reduced density of 1.0, as it crosses the freezing and melting lines, in equilibrium and under constant strain.
 [DOI: 10.1063/1.1683073]

I. INTRODUCTION

The changes in structure and transport in dense monatomic Lennard-Jones (LJ) systems with an isochoric or isobaric decrease in temperature across the liquid–solid transition have been studied since the early times of molecular simulations. Different aspects of the transition have been investigated. The change in diffusion coefficient and the character of collective modes in rapidly quenched amorphous systems,[1,2] the thermodynamics of the glass transition,[2] second peak splitting in the pair distribution function upon quenching or crushing reminiscent of metallic glasses,[1,3] structural analysis of the ordering transition depending on the cooling rate,[4] temperature- and density-dependent structural relaxation,[5] and transition kinetics between local minima on the potential energy hypersurface[6,7] are just some of the examples of explored topics. In all of the works the emphasis has been on characterization of supercooled liquid or ''glassy'' states.

The response to the steady shear of all phases appearing along the isochore has also been extensively explored. It is now well known that even simple liquids like monatomic LJ liquids would shear thin when the strain rate exceeds the Newtonian limit.[8] Subjected to shear, a crystal melts through a series of intermediate phases.[9,10] In glasses, shear stress causes devitrification similar to an increase in temperature,[11] leading to the strain–temperature superposition principle and the definitions of equivalent shear-rate-dependent temperature under deformation. The stress–strain relationship in the elastic domain has been studied for LJ crystals at various state points.[12] Each of these studies was performed at different temperatures and pressures (densities) and with a variety of system sizes.

The aim of this work is to calculate the structural, thermodynamic, and transport properties of the liquid and solid branches of the system of $N=500$ LJ atoms along a high-density isochore in a systematic manner. The equilibrium and nonequilibrium molecular dynamics methods used in this work are explained in the next section. After that, we give an overview of properties of the system without strain (Sec. III). In Sec. IV we compare them to the results for the same system under constant strain generated either with a very high or very low strain rate.

II. SIMULATION METHOD

The Lennard-Jones pair interaction potential Φ_{ij} is given by

$$\Phi_{ij}(r_{ij})=4\varepsilon[(\sigma/r_{ij})^{12}-(\sigma/r_{ij})^{6}], \tag{1}$$

where r_{ij} is the distance between the particles i and j, σ is the exclusion diameter, and ε is the depth of the potential well. Throughout the paper we use the LJ reduced system of units,[13] where σ is the unit of distance, ε is the unit of energy, and mass is measured in units of particle mass.

The system under investigation has the reduced density $\rho=1.0$, which corresponds to an argon density of 1.68 g/cm^3 (Ref. 14). At this density the mean separation of nearest neighbors is incidentally equal to $2^{1/6}$, the position of the energy minimum of the potential (1). Energy and forces have been evaluated within the cutoff distance of 2.5, which contains the first three shells of neighbors. We used the long-range corrections for energy and pressure[13] to compensate for interactions outside the cutoff.

The reduced temperature ranged from 0.7 to 2.0, which corresponds to the range between 84 and 240 K in the case of argon. The reduced freezing and melting temperatures at this density were estimated by interpolation of the phase diagram of Agrawal and Kofke[15] to be 1.46 and 0.931 (175 and 112 K for argon), respectively. The lowest temperature of 0.7 is close to the estimate of the LJ ''glass transition'' temperature (the temperature at which structural arrest occurs due to vanishing of the diffusion coefficient) in the normal-mode theory.[16]

It should be noted that the phase diagram in Ref. 15 has been obtained for an LJ system of similar size as ours, but truncated at half the simulation box length (i.e., at $\sim 4\sigma$ at a density of 1.0, instead of 2.5σ). The liquid–solid part of the phase diagram is not well known for the LJ potential truncated at 2.5σ. It has been shown[17] that the cutoff distance changes the liquid–vapor coexistence curve, especially in the vicinity of the critical point, but there is no estimate of the extent of the change for the liquid–solid coexistence. Therefore the melting and freezing temperatures in all our figures are only approximate—they do not correspond to exactly the same forms of the LJ interaction.

The equilibrium molecular dynamics simulations were performed at constant temperature using the Gauss thermostatting method,[18] which constrains the kinetic temperature

of the system, given by equipartition theorem, to an exact constant at all times. The equations of motion for the positions $\mathbf{r}_i$ and momenta $\mathbf{p}_i$ $(i=1,...,N)$ in equilibrium are

$$\dot{\mathbf{r}}_i=\mathbf{p}_i/m, \quad \dot{\mathbf{p}}_i=\mathbf{F}_i-\alpha\mathbf{p}_i, \tag{2}$$

where $\mathbf{F}_i$ is the total force on particle i arising from the potential (1) and $\alpha=\Sigma_{j=1,N}\mathbf{p}_j\cdot\mathbf{F}_j/\Sigma_{j=1,N}\mathbf{p}_j^2$ is the thermostat multiplier.

The choice of thermostatting method does not affect the equilibrium properties of the system.[19] The equations of motion were integrated using a fifth-order Gear predictor–corrector algorithm, using a time step of 0.001 time units. For liquid states at temperatures above freezing ($T=2.0$ and 1.7) and for all states in the solid branch, the initial configuration was started from the fcc lattice. For the liquid branch close to and below freezing ($T\leqslant 1.5$) the equilibrated liquid configurations at $T=2.0$ were quenched to the desired temperature in one step by simple velocity rescaling. The system was first equilibrated at the desired temperature for 10^7 time steps, and the averages were collected during subsequent 10^7 time steps.

The diffusion coefficient D was computed from the slope of the mean-square displacement (msd) using the Einstein formula

$$\langle r^2(t)\rangle=6Dt, \tag{3}$$

and from the Green–Kubo relation

$$D=\frac{1}{3N}\int_0^{t_w}\sum_{i=1}^{N}\langle\mathbf{v}_i(t)\cdot\mathbf{v}_i(0)\rangle dt, \tag{4}$$

where $\mathbf{v}_i$ is the velocity of particle i, t_w is the time window for the evaluation of the correlation function, and the angular brackets denote the ensemble average. The time window is chosen with the requirement that the correlation function effectively vanish at $t=t_w$. The Green–Kubo formalism was also used for evaluation of the viscosity η and thermal conductivity λ:

$$\eta=\frac{V}{k_BT}\int_0^{t_w}\langle P_{xy}(t)P_{xy}(0)\rangle dt, \tag{5}$$

$$\lambda=\frac{V}{k_BT^2}\int_0^{t_w}\langle\mathbf{j}_q(t)\cdot\mathbf{j}_q(0)dt\rangle dt, \tag{6}$$

where V is the volume of the simulation box and k_B is the Boltzmann constant. In the expression for viscosity, Eq. (5), P_{xy} is the xy off-diagonal element of the stress tensor. In the expression for thermal conductivity, Eq. (6), $\mathbf{j}_q$ is the heat flux vector. In all cases (4)–(6), the time window was chosen as 10^4 time steps.

The isotropic nature of a liquid permits the use of a more general form[20] of Eq. (5) where fluctuations in all components of the traceless symmetric stress tensor are taken into account.

In a partially (e.g., polycrystalline) or fully (e.g., equilibrium or strained crystal) ordered state both viscosity and thermal conductivity depend on the direction with respect to the direction of the crystal axes or the direction of the partial order. Generally, there are several independent values of η and λ, their number dependent on the degree of structural symmetry. Expression (6) is rotationally invariant and can serve as an estimate of the average thermal conductivity. In the strained crystal we evaluated the viscosity associated with the autocorrelation of the off-diagonal elements of the stress tensor, P_{xy}, P_{yz}, and P_{xz}. In the strained crystal we calculated only the decay of the autocorrelation function of P_{xy} in order to compare it to the equilibrium form.

In equilibrium, the pressure tensor is a second-rank isotropic tensor with elements

$$P_{\alpha\beta}=P\delta_{\alpha\beta},$$

where P is the hydrostatic pressure, α and β are the Cartesian directions, and $\delta_{\alpha\beta}$ is the Kronecker symbol. If some of the off-diagonal elements are nonzero or if the diagonal elements are not equal, it means that some internal stresses do not relax and that at least one of the viscosities of such a structure is infinite. We monitored the evolution and averages of all the stress tensor elements in order to detect any unrelaxed stresses.

After establishing the equilibrium properties along the isochore, we perform a simulation equivalent of a rheological relaxation experiment where a specimen is subjected to an instantaneous fixed deformation and study the decay of the stress necessary to maintain this deformation. The strain in the simulation is not in fact applied instantaneously, but the system is instead subjected to a very high strain rate until the desired strain is reached. The dependence of the final state after stress relaxation on the strain rate used to obtain the deformation is also studied.

The system was put under strain using thermostatted Sllod equations of motion with the appropriate periodic boundary conditions:[18]

$$\dot{\mathbf{r}}_i=\mathbf{p}_i/m+\mathbf{e}_x\gamma r_{yi}, \quad \dot{\mathbf{p}}_i=\mathbf{F}_i-\mathbf{e}_x\gamma p_{yi}-\alpha\mathbf{p}_i, \tag{7}$$

where $\mathbf{e}_x$ is the unit vector in the x direction, γ is the strain rate, and the thermostat multiplier in this case has the form $\alpha=\Sigma_{j=1,N}(\mathbf{p}_j\cdot\mathbf{F}_j-\gamma p_{xi}p_{yi})/\Sigma_{j=1,N}\mathbf{p}_j^2$. In order to create strains we used either the strain rate $\gamma=10$ or, for comparison, a low strain rate $\gamma=0.001$.

The values of transport coefficients in principle depend both on system size and on the cutoff distance. Although the mean effect of the truncation on energy and pressure is taken into account in the long-range corrections, the fluctuations in forces change with the cutoff and modify the fluctuations in positions and velocities in the Green–Kubo integrals.[21] The change in transport coefficients due to the cutoff has been shown to be negligibly small close to the LJ triple point,[22] but may be more significant in the liquid–solid transition region. Therefore, strictly speaking, the transport coefficients and freezing–melting temperatures do not correspond to the same LJ model and the same caution applies as for thermodynamic properties.

III. EQUILIBRIUM SYSTEM

A. Static properties

At $T=2.0$ the system is in a purely liquid state. As the temperature is lowered along the isochore towards the freez-

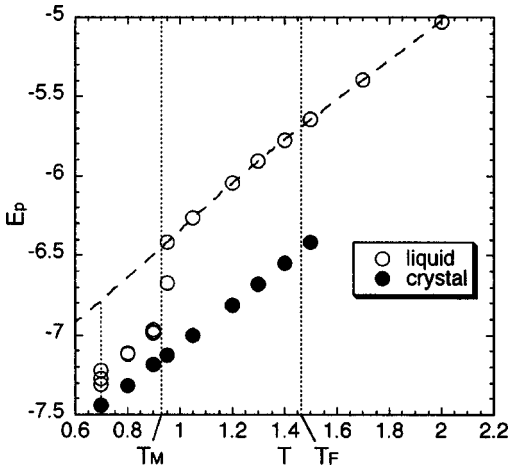

FIG. 1. Dependence of the potential energy per particle on temperature for the crystal and liquid states at constant density. "Liquid" below the melting temperature T_M is in fact an instantaneously quenched liquid after relaxation to a polycrystalline solid. The dashed line is an extrapolation to the supercooled liquid potential energy, which is equal to -6.8 at $T=0.7$. The error bars are negligible on this scale.

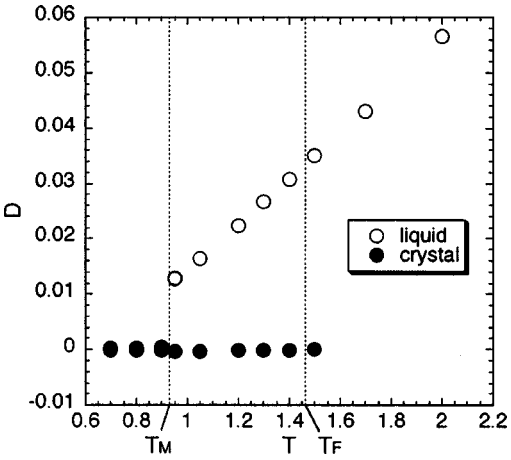

FIG. 2. Dependence of the diffusion coefficient on temperature in liquid and solid phases. In the quenched supercooled polycrystalline states below T_M, the diffusion coefficient does not in fact vanish, but is indistinguishable from the zero solid value on this scale. The error bars are negligible on this scale.

ing temperature ($T \leqslant 1.5$), both the fcc crystal and liquid phases become stable. There is no coexistence region because the system size is too small to allow the formation of an interface. Below the melting temperature, the liquid freezes very quickly (in around 10^4 time steps) into a partially ordered polycrystalline state. The structure of this supercooled state is randomly stacked close packed with many defects.[1,4] For each submelting temperature we produced three different supercooled structures by the quenching of three different configurations of the liquid at $T=2.0$. The pair distribution of the three supercooled states in all cases had similar short-range structure, with the same splitting of the first peak, much less pronounced than in the fcc lattice, and much less structure in the subsequent peaks. By examining the projections of the particle positions onto three different planes, we found that these structures are quite stable, with the unchanged overall appearance after 2×10^7 time steps. This was confirmed by their unchanging potential energies and stress tensor elements.

The transition is in fact crystallization caused by a small system size and periodic boundary conditions.[22] Since the structure has many defects, the crystallization is only partial and the system is not fully equilibrated, therefore having many common features with glasses.

In the coexistence region there is hysteresis in the potential energy and pressure (Fig. 1) between the solid and liquid branches. Both energy and pressure are lower in the fcc solid than in the liquid. In polycrystalline states they closely approach the fcc crystal values. This effect is analogous to the hysteresis in volume observed during the isobaric liquid–solid phase transition.[4]

B. Dynamic properties

At densities close to the triple-point density the diffusion coefficient decreases linearly with temperature[19] (Fig. 2). The same trend is observed in the liquid phase of our system all the way to the melting temperature. Below melting, when the liquid freezes rapidly into a defective polycrystal, there is a sharp drop in the diffusion coefficient.

The liquid velocity autocorrelation functions typically show a change of sign and a pronounced minimum, followed by a negative plateau and a negative tail.[23] This shape is observed in the whole range of temperatures between 2.0 and 0.95 in the liquid state. At liquid densities (e.g., close to the triple-point density) the first collision comes before the neighbors have time to form a vortex, so there is an enhanced backscattering manifested by the change of sign. Further enhancement of the forward motion at later times is lost in noise and is undetectable.

More velocity reversals become visible in the quenched polycrystals below melting. In this region the time integral drops two orders of magnitude, but still does not vanish because of the motion of defects. In a crystal, the positive and negative contributions cancel at long times, resulting in a vanishing diffusion coefficient.

For temperatures down to 0.95 just above melting, inspection of the time dependence of the mean-square displacement as a function of temperature shows at first a linear increase of the msd with time characteristic of liquids. For quenched polycrystals at lower temperatures (below melting) there is a qualitative change of shape of the msd evolution—at first there is a sharp increase and a maximum reminiscent of the solid msd, followed by a very slow but unmistakable lightly modulated linear increase. Rahman *et al.*[1] observed a similar effect after quenching to a much lower temperature ($T=0.108$), but in much shorter runs after quenching (10^5 time steps), before the system reached the metastable equilibrium. This is consistent with the existence of short-lived phonons: a particle is undergoing oscillatory motion within walls of a cage of nearest neighbors until a momentary structural breakdown permits its escape to a new cage.

In a crystal, the mean-square displacement converges to a constant proportional to the average squared amplitude of oscillations around the crystal sites. This constant increases

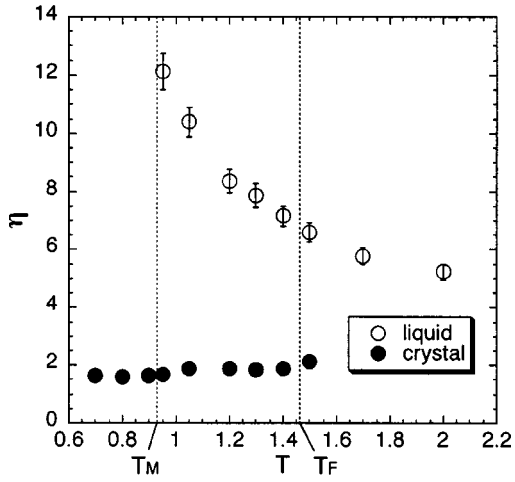

FIG. 3. Viscosity of a liquid increases with the decrease in temperature and diverges at melting temperature T_M. "Viscosity" of a crystal is much lower than in a liquid and decreases with the decrease in temperature. However, its meaning is different than in a liquid. The statistical error in viscosity calculations is ~6%.

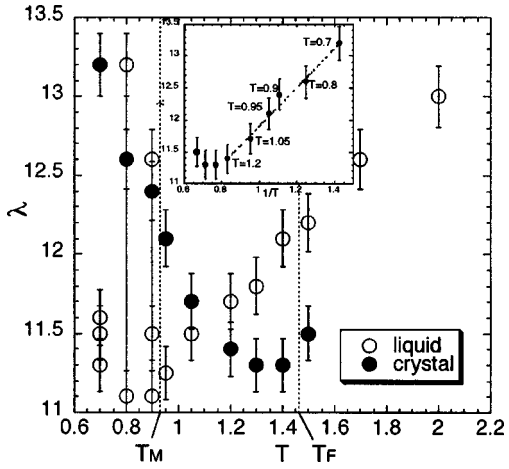

FIG. 5. Dependence of thermal conductivity on temperature in liquid and solid phases. In the liquid phase the thermal conductivity steadily decreases with temperature. In a crystal the trend is the opposite, with the thermal conductivity proportional to the inverse temperature up to $T=1.2$ (inset), in accordance with the phonon perturbation theory. Different polycrystalline structures below T_M have very different values of λ. Statistical error is ~2%.

nearly linearly with temperature, implying that the potential felt by the particles is very nearly harmonic for all states where the crystal is stable.

The liquid branch viscosity increases with the decrease in temperature and diverges close to the melting temperature (Fig. 3), mostly due to the increase in relaxation time.

The viscosity in the solid (crystal) is infinite by definition: a crystal does not flow. However, in equilibrium the average values of the off-diagonal elements of the stress tensor vanish, and the average diagonal elements are equal because there is no internal stress. Therefore the integrand of Eq. (5) converges to zero (Fig. 4) and the integral has a finite value. The shear stress autocorrelation function has modulations caused by elastic waves of higher amplitude and longer lifetime as the temperature decreases, superimposed upon a form similar to that of a liquid. The value of the integral is much lower than the liquid viscosity at the same temperature (Fig. 3).

In a crystal, fluctuations of particles around lattice sites can be regarded as flow on a short time scale. Their motion causes instantaneous local strains and internal stresses. As a consequence, local flow velocity profiles develop in order for the stresses to relax, and the viscosity present in the integral (5) governs the relaxation of some directions of these flows. The viscosity of a solid is lower than in a liquid because the fluctuations of shear stress are much smaller in a crystal than in a liquid and shear stress relaxes faster.

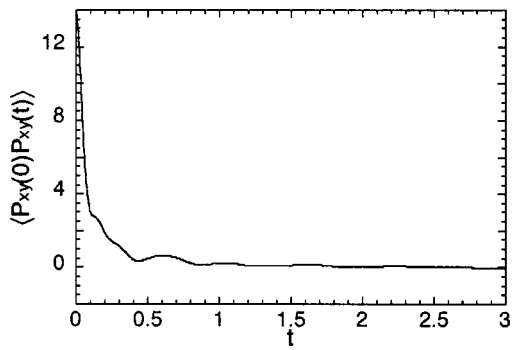

FIG. 4. Shear stress autocorrelation function of an ordered crystal at $T=0.7$. Shear stress has zero average, and one observes long-lived phonon excitations.

When liquid crystallizes into defective polycrystals, its viscosity diverges. This is of the same origin as the drop in the diffusion coefficient—when particles become "trapped" and their motion limited, the internal strains and stresses relax too slowly to show on the simulation scale. The stress relaxation still shows some vibrational excitations, but attenuated by anharmonic phonon interactions caused by structural defects. The "final" internal stress cannot be predicted from the stress fluctuation in the initial quenched state. The same general behavior is also expected in a glassy state.

The thermal conductivity in liquid and solid phases is not strongly temperature dependent—the total change in the whole temperature range does not exceed 15% (Fig. 5). The thermal conductivity of a liquid consists of a diffusive contribution and of a contribution due to an isotropic interaction. It decreases almost linearly with the decrease in temperature until the melting transition is approached, where it decreases faster. This trend suggests that the heat conduction in a liquid is mostly a diffusive effect. The heat flux relaxation times are similar and very short in the whole temperature range (around 500 time steps), and the decrease in conductivity is mainly a result of the decrease in fluctuation amplitudes.

In contrast to the liquid behavior, in an ordered crystal the heat flux propagates exclusively because of elementary excitations. The contribution of phonon interactions is contained in the interaction term of the heat flux, while the diffusion contribution vanishes.[24] When the anharmonic interaction is small and the phonon lifetime is many vibrational periods (low-temperature approximation), the perturbation theory approach is valid and yields phonon lifetimes and thermal conductivity inversely proportional to temperature.[25]

For soft (r^{-12}) potentials this behavior is valid up to half the melting temperature.[24] In our system the inverse temperature dependence is obeyed up to $T=1.2$—i.e., for much higher temperatures than the soft system (inset in Fig. 5). The reason for this is probably that at this density the LJ potential is the most harmonic.

For the polycrystalline state below the melting temperature there is a large spread in thermal conductivity values. The average mobility in a particular state determines the diffusive contribution. The degree of partial order determines the anharmonicity of the average particle potential, which decreases the phonon lifetimes and the phonon contribution to thermal conductivity.

IV. STRAINED SYSTEM

A. Liquid

Liquids cannot support strain for a long time. However, when they are deformed suddenly, for a short time they behave like an elastic solid. In this case the maximum stress at the end of the deformation is proportional to strain. In a simulation, if the total displacement in the x direction of the first upper row of neighbor cells (images with coordinates shifted by L in the y direction) is equal to δ, the dimensionless strain ε is equal to δ/L, and it is proportional to the value of the P_{xy} element of the stress tensor at the end of the deformation process $P_{xy}^{\max}$,

$$\varepsilon = -GP_{xy}^{\max}, \tag{8}$$

where G is the shear modulus of the liquid (Fig. 7). In an ''ideal'' viscoelastic liquid described by the Maxwell model of viscoelasticity,[26] the liquid shear modulus exists only for an instantaneous deformation. In reality, the linear relationship (8) will be valid as long as the time of deformation is small compared to the shear stress relaxation time. In Fig. 6(a) we show the shear stress at the end of the deformation generated by the strain rate $\gamma=10$ for large strains ranging from 0.1 to 1.0 at temperatures of 1.05 and 2.0. At lower temperature the shear stress relaxation time (determined from the decay of the stress autocorrelation function to be approximately 6500 time steps) is sufficiently longer than the time of deformation (the strain of $\varepsilon=1$ was generated during 100 time steps), so that the instantaneous shear stress response is elastic for all but the largest strain. At higher temperature, the relaxation time is approximately 10^3 time steps and one can see deviations from the linear dependence for strains that took more than 2% of this time to generate. The maximum shear stress is lower than predicted by the linear relationship (8) because the relaxation process has reduced the stress before the deformation process has finished [Fig. 6(b)].

The ''shear strength'' of a liquid (the maximum strain for which an instantaneous response is elastic) decreases with temperature, but the shear modulus G for a ''sudden'' deformation slightly increases. Assuming that the decay of the shear stress autocorrelation function can be represented by a single exponential (Maxwell model of viscoelasticity), the ''instantaneous'' or infinite-frequency shear modulus can be estimated from the fluctuations of the shear stress:

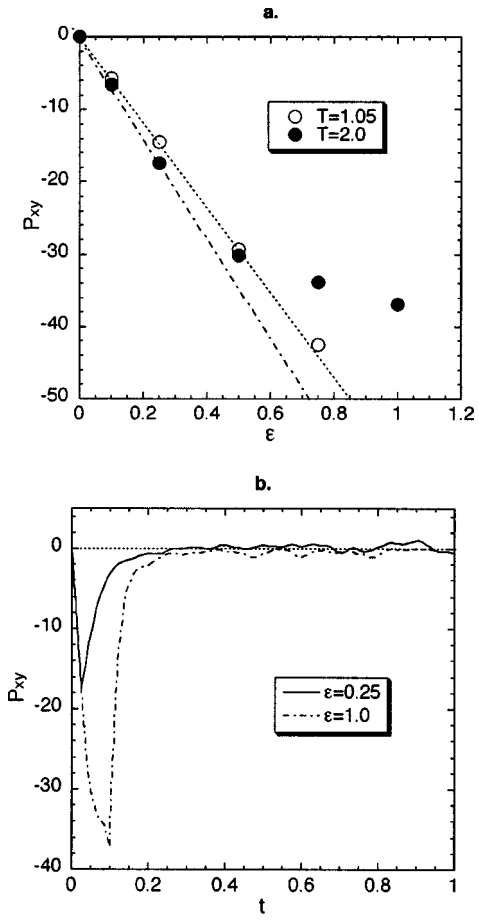

FIG. 6. (a) Dependence of shear stress at the end of deformation generated with the strain rate $\gamma=10$ on final strain in a liquid at two temperatures. The dependence is linear for a larger range of strains at the lower temperature. (b) Increase of shear stress under deformation of a liquid at $T=2.0$ and its relaxation when the deformation process is completed. If the deformation time is sufficiently long (larger strain $\varepsilon=1.0$), the stress relaxation begins before the end of the deformation. The error bars are negligible on this scale.

$$G=\langle P_{xy}^2\rangle/k_BTV. \tag{9}$$

This expression provides a good estimate, showing the same trend of increase with temperature as the linear fit of the simulation data in Fig. 7(a). At $T=1.5$, we obtain $G=57.4$ from a linear fit and $G=52.2$ from Eq. (9). At $T=2.0$ the linear fit gives $G=69.7$, while the estimate from Eq. (9) is $G=66.2$.

The effect of the relaxation time can be seen if the same deformations are generated at constant temperature by successively lower strain rates [Fig. 7(a)]. The shear stress at the end of deformation obeys the same linear relationship (8) with the same shear modulus irrespective of the strain rate while the total time of deformation is sufficiently smaller than the relaxation time. Since the time of deformation increases with the decrease in strain rate, the liquid behaves elastically for a narrower range of strains as the strain rate decreases.

When the deformation is completed, the relaxation process begins. While the work done in straining the liquid is extracted to the heat bath, the energy, pressure, and shear stress return to their equilibrium values. The decay of the shear stress causes the decay of the shear modulus [Fig.

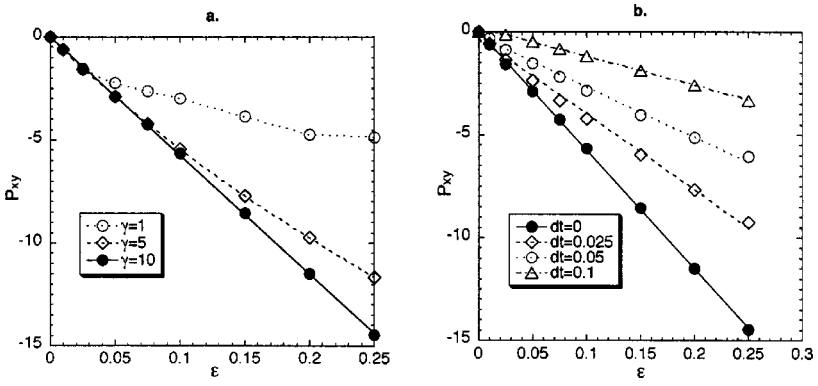

FIG. 7. (a) Shear modulus does not depend on the strain rate used to generate strain, but the region of elasticity of a liquid becomes narrower as the strain rate decreases. The solid line is a linear fit, whereas the dashed lines are for eye guidance only. (b) Decay of the shear modulus in time (*dt* is the time after deformation). Data are for the liquid at $T=1.05$. The error bars are negligible on this scale.

7(b)]. In the elastic strain range the shear stress decays at the same rate for all strains, so that the linear relationship (8) is satisfied at all times, but with the value of the shear modulus G decreasing in time. As expected, the transport coefficients D, η, and λ and the corresponding time-correlation functions in the relaxed state with strain are the same as in equilibrium.

The supercooled liquid state at $T=0.95$ did not crystallize in equilibrium, but showed all the liquid-state characteristics: liquidlike pair distribution function without peak splitting, diffusion coefficient several orders of magnitude larger than in the polycrystalline state, and no unrelaxed stresses and therefore finite viscosity. After applying strain, the increased potential energy and the induced shear stress decayed to equilibrium values, but shortly afterwards the liquid crystallized into different polycrystals. This result is in accordance with the view that in a supercooled liquid an external disturbance promotes the liquid–solid transition. The final state depended sensitively on the imposed strain and strain rate at which the deformation was generated. There was no simple relationship between the unrelaxed shear stress in the final polycrystalline state and the imposed strain.

B. Solid

Small deformations of solids are reversible or elastic—they disappear in the absence of applied stress. In the elastic domain shear stress is proportional to strain. Strains superior to the elastic limit are neither linear nor completely reversible; they are plastic. If the solid is deformed further, it reaches the fracture point, where the change of stress with strain is discontinuous.

A simple theory of Frenkel,[27] which considers the stability of only two periodic layers of atoms in a sinusoidal effective potential sliding past each other, predicts failure at the strain of $\varepsilon=0.25$. In reality, solids like metals become plastic for deformations at least two orders of magnitude smaller. The shear modulus and the limit of elasticity is not known for van der Waals solids like argon, but the elastic constants have been evaluated in computer experiments[12] for very low temperatures $T\leqslant 0.5$.

We measured the strain–stress relationship for a large range of deformations (up to $\varepsilon=0.35$) of the crystal at $T=0.7$, where only the solid phase is stable [Fig. 8(a)]. One set of results was obtained for strains created with a very high strain rate ($\gamma=10$, ''sudden deformation''), the other with a computationally very low strain rate ($\gamma=0.001$) applied in the x direction—i.e., the [100] direction of the fcc crystal.

Under sudden deformation, the magnitude of the shear stress increases rapidly in proportion to strain [partially shown as crosses in Fig. 8(a)], but starts to decay to a lower value as soon as the deformation is completed. During deformation, the (100) planes become tilted in the direction of

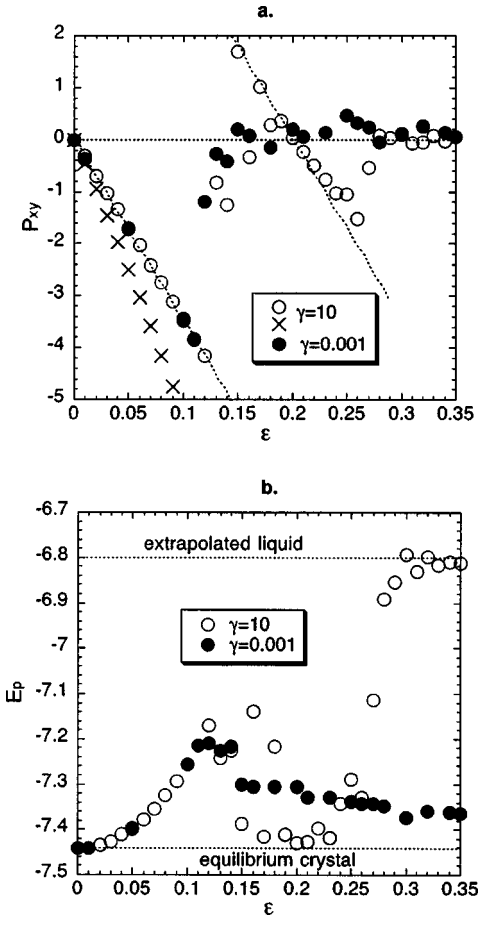

FIG. 8. Deformation of a crystal at $T=0.7$. (a) Stress–strain relationship for the maximum stress at the end of deformation (crosses) and after relaxation (open circles) created with strain rate $\gamma=10$ and created with $\gamma=0.001$ after relaxation. (b) Dependence of the relaxed potential energy on strain. In the elastic region error bars are negligible. For strains $\varepsilon>0.12$ the results are shown for one run only, but are expected to have a larger spread depending on the nature of defects.

shear without any rearrangement of atoms in the planes. Shear stress relaxes by in-plane reorganization after deformation is completed. In the elastic region up to $\varepsilon=0.11$ relaxed shear stress is proportional to strain and independent of the strain rate with which the deformation had been generated. The shear modulus is equal to $G=34.8$, not far from the value of 41.3 obtained in Ref. 16 at $T=0.5$. In this region, the potential energy as a function of strain [Fig. 8(b)] has a harmonic form. The large region of elasticity is caused by the small system size in periodic boundary conditions that enhance the crystal stability and the particular choice of density.

As the strain increases beyond $\varepsilon=0.11$, there is fracture and the configuration relaxes to different forms of polycrystals consistent with periodic boundary conditions, depending on the strain rate.

For fast deformation above $\varepsilon=0.15$ the relaxed stress reverses sign and there is another almost elastic region up to $\varepsilon=0.24$. The sign reversal means that, although the strain was generated by shearing the crystal in the positive x direction, one ultimately has to apply stress in the negative x direction to sustain the deformation. The origin of this effect is in the periodic boundary conditions. The simulation box consists of five rows and five columns of elementary fcc cells containing four atoms each. If the top and bottom simulation boxes slide by 0.2 cell lengths, one of the crystal forms consistent with the periodic boundary conditions is the original unstrained fcc lattice. The strain of 0.15 can alternatively be obtained by straining the $\varepsilon=0.2$ unstrained lattice in the negative direction by 0.5—the evidence of this is the fact that the shear stress at $\varepsilon=0.15$ is equal in magnitude and of opposite sign to the shear stress at $\varepsilon=0.5$. If the external stress were removed, this configuration would relax in the positive x direction to the unstrained configuration at $\varepsilon=0.15$. The mechanism of shear stress reversal, as shown in Fig. 9, is the rearrangement of atoms in several tilted planes and diffusion between them. This combination of dislocations propagates through the crystal until a configuration with reversed stress is attained. At $\varepsilon=0.2$ shear stress indeed nearly vanishes and the potential energy is very close to the equilibrium crystal energy. The small discrepancies are the result of defects in this ''secondary'' fcc structure.

For the fast deformation of $\varepsilon=0.3$ and larger, shear stress vanishes after relaxation of around 5×10^3 time steps. Inspection of the potential energy [Fig. 8(b)] shows that in this case the configuration is not that of an unstrained crystal, but that the solid completely melts during relaxation. The potential energy is in fact equal to the liquid potential energy extrapolated to the submelting temperature of 0.7. If equilibration is continued for around 10^6 more time steps, the liquid eventually freezes into a strained polycrystal.

When the crystal is deformed slowly ($\gamma=0.001$, solid circles), most of the rearrangement and shear stress relaxation take place during deformation. For strains outside the elastic domain there is no secondary elastic region, because the crystal undergoes structural changes during deformation and relaxes from configurations completely different from the rapidly strained lattice (Fig. 10). The potential energy never reaches the extrapolated liquid value. The crystal never melts, but undergoes a sequence of fractures and rearrangements into strained polycrystals.

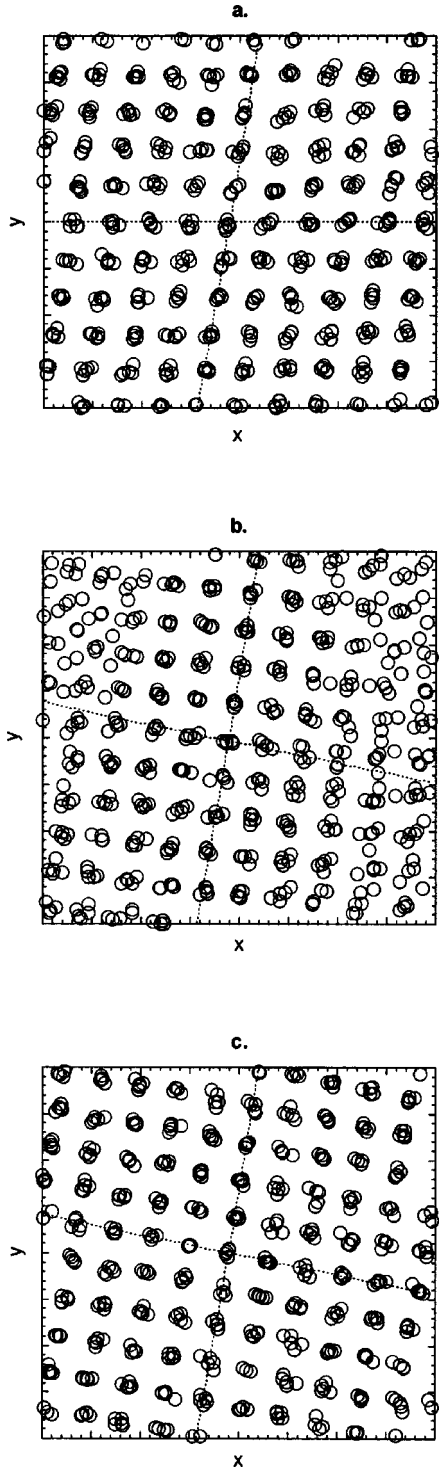

FIG. 9. Rearrangement after fast deformation at the strain of 0.15: (a) 2.5 time units after deformation, (b) 5×10^3 time steps after deformation, and (c) 10^4 time steps after deformation.

For the crystal at increased temperature $T=1.2$—i.e., in the liquid—solid coexistence part of the phase diagram—there is again a range of strains for which the crystal is elastic. The shear modulus $G=32.3$ is less than 10% lower than at $T=0.7$; it is not very sensitive to the changes in temperature. Shear strength decreases: the linear elastic region ends

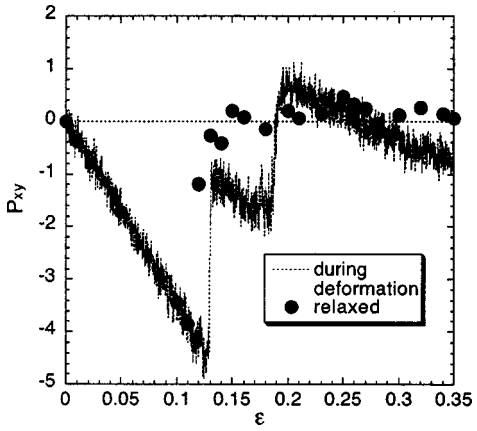

FIG. 10. Change of shear stress during a slow deformation $\gamma=0.001$, depending on instantaneous strain $\varepsilon(t)$. For comparison, solid circles represent the shear stress at corresponding strain obtained with the same strain rate after relaxation.

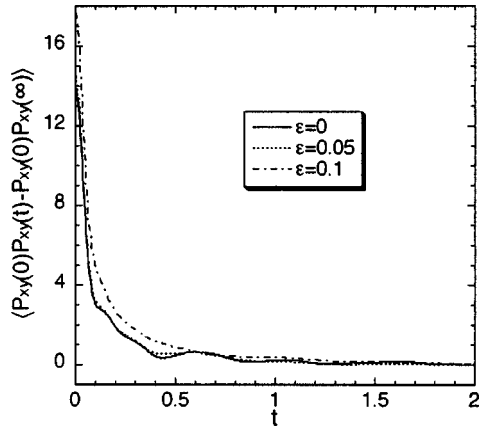

FIG. 11. Decay of the shifted shear stress correlation function [Eq. (10)] in equilibrium and strained crystals in the elastic region at $T=0.7$.

at $\varepsilon=0.08$ and is followed by a nonlinear plastic region up to $\varepsilon=0.1$, where differences between shear stresses at the same strain obtained with different strain rates start to appear. For higher strains there is failure with relaxation to defective polycrystalline states, similar to the low-temperature crystal. However, there is no secondary ''mirror image'' elastic region, and for fast deformations above $\varepsilon=0.15$ the crystal melts. Because of the small system size, the liquid does not recrystallize later. Again, for deformations obtained with low strain rate there is no melting, but only a sequence of fractures. The results at higher temperature are just an indication of the qualitative change of the stress–strain relationship with the increase in temperature. Otherwise, much is an artifact of the small system size. In reality, in this state there are not two stable phases, but two phases in coexistence having an interface, and the impact of strain would be completely different.

The transport properties of a crystal under strain are different from their values in an unstrained crystal. The diffusion coefficient slightly increases from zero because of the presence of defects. The viscosity evaluated from the integral of the shear stress correlation function (5) is infinite because there is a finite average shear stress. However, we can evaluate the ''effective viscosity''

$$\eta^*=\frac{V}{k_BT}\int_0^\infty [P_{xy}(t)P_{xy}(0)-P_{xy}(\infty)P_{xy}(0)]dt, \quad (10)$$

which gives the internal friction associated with the ''flow'' of atoms around the strained lattice sites in the [100] direction. In analogy with the viscosity of the equilibrium crystal shown in Fig. 3, it describes the decay rate of the P_{xy} stress autocorrelation function towards the final relaxed value. The decay of the integrands Eq. (10) in equilibrium and for two different strains is shown in Fig. 11. The initial value at $t=0$ increases with strain—the fluctuations of shear stress around the mean value increase as the average position of particles moves further from the stable equilibrium position. Also, the normal modes (phonons) change as the lattice is deformed. The oscillations of the phonon origin are attenuated as anharmonic interactions increase. All this contributes to an overall increase in the effective viscosity with strain. Similar considerations apply to the dependence of thermal conductivity on strain. The dependence of the effective viscosity η^* and thermal conductivity λ on strain in the elastic region of the crystal at $T=0.7$ is shown in Fig. 12.

V. CONCLUSION

We compared properties of equilibrium and strained liquid and solid branches of the Lennard-Jones system along the $\rho=1.0$ isochore. In the equilibrium system the diffusion coefficient decreases linearly with a decrease in temperature. At the melting temperature there is a sudden drop in diffusion due to crystallization caused by periodic boundary conditions and small system size. Diffusion vanishes in a perfect crystal. Viscosity increases with a decrease in temperature and diverges at the melting temperature, again because of incomplete crystallization. The unstrained crystal has almost constant viscosity of a much lower value than the liquid. Thermal conductivity in a liquid is mostly diffusive and decreases nearly linearly with temperature. In a solid it is due to phonon interactions and increases as the temperature de-

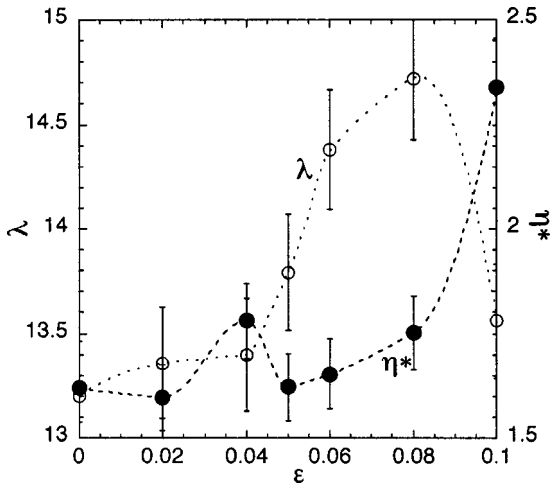

FIG. 12. Dependence of ''effective viscosity'' η^* and thermal conductivity λ on strain in the elastic region at $T=0.7$. Statistical error is ~5% for viscosity and ~2% for thermal conductivity.

creases. At low temperature it is proportional to the inverse temperature in agreement with Peierls theory. The discontinuities in thermodynamic and transport properties occur remarkably close to the melting temperature of the LJ phase diagram for a system with a much larger interaction cutoff, suggesting that the truncation distance does not have a very strong influence on the position of the liquid–solid coexistence region.

The initial shear stress caused by the sudden deformation of a liquid is proportional to strain until the time of deformation is of the order of 1% of the equilibrium shear stress relaxation time. The coefficient of proportionality is the ''infinite-frequency shear modulus,'' which can be estimated from the $t=0$ value of the stress autocorrelation function. The shear modulus decays to zero as shear stress relaxes. In the final relaxed state there is no influence of strain on transport in liquids.

In a solid, for small deformations the relaxed stress is proportional to strain and independent of the strain rate with which it has been deformed. The shear modulus and shear strength weakly decrease with an increase in temperature. For higher strains the deformations become irreversible and depend on the strain rate with which they were created. For a ''sudden deformation'' there is a secondary elastic region, followed by a sequence of rearrangements into defective polycrystals. For even higher strains the crystal completely melts during relaxation and finally recrystallizes after a longer equilibration period. If the deformation is performed slowly, the relaxation starts during deformation. There is no secondary elastic region—only a series of fractures of strained polycrystals.

In the elastic region under strain, the diffusion coefficient is slightly increased due to defects. Viscosity is infinite since the shear stress does not relax. The ''effective viscosity''—i.e., the internal friction during vibrations—increases because the anharmonicity of the effective potential in a strained lattice causes increased fluctuations of shear stress. The change in normal modes in a strained lattice causes also a change of thermal conductivity.

There are two types of artifacts in this simulation. One type is related to the small system size and periodic boundary conditions. It causes rapid crystallization below the melting temperature and the absence of liquid–solid coexistence. It is also responsible for the abnormally high shear strength and wide elastic region. In this sense, our results for the strained crystal are more applicable to thin crystal sheets under strain than to bulk crystal behavior.

The other type of artifact is related to the thermostatting procedure and is most relevant for the stress relaxation part of the simulation after the ''sudden deformation.'' After the deformation is finished, the residual velocity profile is instantly interpreted as heat and attenuated by the thermostat. The use of some profile-unbiased thermostat (PUT), such as a ''configurational temperature thermostat,'' [28] would possibly change the relaxation process and the final structure.

A simulation with a larger system size and a PUT would provide more realistic answers about the shear strength and the existence of the secondary elastic region (reminiscent of stick–slip behavior in thin films) in crystal sheets and in bulk. It would also elucidate the onset of the shear-induced melting of LJ crystals, in particular if there is a threshold strain rate below which there is a sequence of fractures and above which the crystal melts. We plan to address these questions in future work.

ACKNOWLEDGMENTS

The author wishes to thank Jerome Delhommelle, Peter Daivis, Peter Harrowell, Howard Hanley, Denis Evans, and Stephen Williams for helpful discussions. A generous allocation of computer time for this project by the Australian Partnership for Advanced Computing is gratefully acknowledged.

[1] A. Rahman, M. J. Mandell, and J. P. McTague, J. Chem. Phys. **64**, 1564 (1976).
[2] J. R. Fox and H. C. Andersen, J. Phys. Chem. **88**, 4019 (1984).
[3] F. F. Abraham, J. Chem. Phys. **72**, 359 (1980).
[4] S. Nosé and F. Yonezawa, J. Chem. Phys. **84**, 1803 (1986).
[5] C. A. Angell and L. M. Torrell, J. Chem. Phys. **78**, 937 (1984).
[6] F. H. Stillinger and T. A. Weber, Phys. Rev. A **28**, 2408 (1983).
[7] S. Sastry, P. G. Debenedetti, and F. H. Stillinger, Nature (London) **393**, 554 (1998).
[8] D. J. Evans, H. J. M. Hanley, and S. Hess, Phys. Today **37**(4), 27 (1984).
[9] D. J. Evans, Phys. Rev. A **25**, 2788 (1982).
[10] L. W. Woodcock, Phys. Rev. Lett. **54**, 1513 (1983).
[11] I. K. Ono, C. S. O'Hern, D. J. Durian, S. A. Langer, A. J. Liu, and S. R. Nagel, Phys. Rev. Lett. **89**, 095703 (2002).
[12] D. J. Quesnel, D. S. Rimai, and L. P. DeMejo, Phys. Rev. B **48**, 6795 (1993).
[13] M. P. Allen and D. J. Tildesley, *Computer Simulation of Liquids* (Clarendon, Oxford, 1987).
[14] P. Borgelt, C. Hoheisel, and G. Stell, Phys. Rev. A **42**, 789 (1990).
[15] R. Agrawal and D. A. Kofke, Mol. Phys. **85**, 43 (1995).
[16] B. Madan, T. Keyes, and G. Seeley, J. Chem. Phys. **94**, 6762 (1991).
[17] B. Smit, J. Chem. Phys. **96**, 8639 (1992).
[18] D. J. Evans and G. P. Morriss, *Statistical Mechanics of Non-Equilibrium Liquids* (Academic, London, 1990).
[19] D. J. Evans and S. Sarman, Phys. Rev. E **48**, 65 (1993).
[20] P. J. Daivis and D. J. Evans, J. Chem. Phys. **100**, 541 (1993).
[21] J. López-Lemus and J. Alejandre, Mol. Phys. **100**, 2983 (2002).
[22] J. D. Honeycutt and H. C. Andersen, Chem. Phys. Lett. **108**, 535 (1984).
[23] D. Levesque and L. Verlet, Phys. Rev. A **2**, 2514 (1970).
[24] A. J. C. Ladd, B. Moran, and W. G. Hoover, Phys. Rev. B **34**, 5058 (1986).
[25] R. E. Peierls, Ann. Phys. (Leipzig) **3**, 1055 (1929).
[26] N. W. Tschoegl, *The Phenomenological Theory of Linear Viscoelastic Behavior* (Springer-Verlag, Berlin, 1989).
[27] C. Kittel, *Introduction to Solid State Physics, 6th edition* (Wiley, New York, 1986).
[28] J. Delhommelle and D. J. Evans, J. Chem. Phys. **115**, 43 (2001).